Theoretical and Experimental Investigation of Space-Realizable Inertial Actuation for Passive and Active Structural Control

David W. Miller* and Edward F. Crawley†
Massachusetts Institute of Technology, Cambridge, Massachusetts

Inertial reaction devices are investigated for use as passive vibration absorbers and active control actuators for flexible space structures. Absorbers are designed for one- and two-degree-of-freedom structural representations using three parameter optimization techniques. All three yield nearly identical designs and indicate that inertial devices should be tuned to the lowest mode intended to receive increased damping. The optimal passive components of the control actuator are found to be those of the optimal passive vibration absorber. Proof-of-concept laboratory tests were performed on a quasi-free-free beam using inertial reaction devices that are space-realizable, i.e., conceptually capable of functioning in the space environment. The inertial devices were used as both passive absorbers and tuned actuators. Damping was significantly increased using both passive and passive/active techniques. Additional tests indicated the benefits and limitations of actuator tuning and the necessity of performing realistic experiments using space-realizable hardware.

Nomenclature

A = state dynamics matrix
b_i = ith row of control effectiveness matrix
B = control effectiveness matrix
c = damper strength
c_{1i} = ith column of modal measurement matrix
C = regulated variable matrix
d_i = ith row of modal disturbance matrix
D = disturbance effectiveness matrix
D_c = positive definite modal damping matrix
f = feedback gains
F = control force, feedback gain matrix
J = system cost
k_i = stiffness of ith spring
m_i = mass of ith mass
M = measurement matrix
P = disturbance force
Q = quadratic state penalty
Q_D = disturbance torque
R = quadratic control effort penalty
u = nondimensional control force
w = disturbance inputs
x = state vector, displacement
y = regulated variables
z = measured variables
α = positive gain parameter
β = absorber-to-structural modal mass ratio
γ = nondimensional frequency ratio
δ = absorber-to-structure modal frequency ratio
μ = nondimensional damper strength
σ_i = second-order modes for internally balanced system
Φ_{DEC} = decimated eigenvector matrix
ζ_i = damping of ith mode
ω_i = frequency of ith mode

Introduction

A NUMBER of future space structures may require active control of their flexible modes. Because of the lack of passive energy dissipation mechanisms in space, even small disturbances can lead to motions of sufficiently large amplitude or duration as to be detrimental to performance requirements. A two-level approach to controlling structural vibrations is envisioned. First, the background structural and material damping can be increased by addition of passive damping devices. Second, an active control system can be added to further enhance system performance. In this scenario, the purpose of the passive damping device is threefold: to provide a supplementary passive dissipation mechanism, to increase the robustness of the active system, and to provide a fallback in the event of failure of some or all of the active system.

Several options are available for introducing passive damping and active control into the structural dynamics. Passive energy dissipation mechanisms that can be implemented in space include material damping enhancement, viscoelastic dampers, frictional dampers and joints, intermember dampers, and inertial reaction absorbers. Mechanisms for active damping include piezoelectric devices, interelement actuators, angular momentum exchange devices, and inertial reaction actuators. Common to the list of options for passive dissipators and active actuators are inertial reaction devices. These are conceptually simple devices that are easily implemented in space. Questions associated with such devices include their theoretical optimization and experimental implementation.

Previous investigations have addressed the theoretical optimization of passive absorber designs. The classical single-degree-of-freedom (DOF) vibration absorber solution[1] is well-known and has found wide application. Recently a closed-form solution was derived, based on a quadratic regulator formulation, that yields the same design for a one-DOF absorber.[2] Currently these devices are commonly used to damp structures that respond primarily in a single mode of vibration. This work will extend their application to the damping of two-DOF structures and will examine their performance in structures with multiple modes. The incorporation of vibration absorbers as the passive components of active inertial control actuators will also be examined.

Inertial reaction actuators are conceptually capable of functioning in the space environment, i.e., they are space-realizable. One practical implementation of an inertial reaction actuator is the pivoted proof-mass actuator currently being considered for use in active vibration suppression.[3] The work presented here makes use of similar devices but incorporates tunable passive components into the design of active control

Received Aug. 1, 1986; revision submitted Jan. 27, 1987.

*Research Assistant, Department of Aeronautics and Astronautics, Space Systems Laboratory. Member AIAA.

†Associate Professor, Department of Aeronautics and Astronautics, Space Systems Laboratory. Member AIAA.

actuators for the implementation of low-authority control.[3,4] A distinction of the experiments described herein is that no actuating or sensing is performed against the laboratory frame. This work focuses on the use of tunable inertial reaction devices that operate through momentum exchange between the structure and a reaction mass to perform output feedback control.[5]

This paper is divided into two main sections dealing with the issues of theoretical optimization and experimental implementation. First, the components of a passive inertial vibration absorber and the passive components of an inertial control actuator are optimized. The passive absorber (Fig. 1a) consists of a spring, mass, and damper. With the addition of a feedback control force F in parallel, the device becomes an active control actuator. Because of the functional similarities in the inertial absorber and actuator models, both concepts can be combined into one physical device. The availability of adjustable passive parameters allows the passive and active characteristics of the actuator to complement each other. The absorber and actuator are optimized by several criteria including minimum steady-state response, minimum modal time constant, and quadratic cost minimization.

In the second part of this paper, experiments are used to identify practical approaches and limitations in the use of these devices. First, the actuators are experimentally tuned to beam modes as absorbers. Once tuned, these devices are used as control actuators. A control test is performed using actuators without optimized passive characteristics in order to demonstrate that improved performance is achieved when the actuators are tuned. Finally, a test involving actuation against the laboratory frame is used to demonstrate the relative ease of gaining deceptively high performance with non-space-realizable devices.

Optimization of Passive Absorber Parameters

The passive inertial vibration absorbers are first optimized for the systems shown in Fig. 1. In Fig. 1b the absorber (m_2, k_2, and c) is attached to a single-degree-of-freedom spring/mass system (m_1 and k_1) that represents the modal stiffness and modal mass of one structural mode. Figure 1c is the model used for optimizing the absorber to a two-DOF plant. The force P indicates the location of an assumed input disturbance on the structure.

Three different approaches are used to determine the optimal spring and damper values for the passive vibration absorber. First, a steady-state minimax criterion is used to select parameters that minimize the maximum steady-state structural response. Second, a set of absorber parameters is chosen which places the system poles such that the maximum modal time constant is minimized. A third optimal solution is found by minimizing a weighted quadratic cost integral of the response. The steady-state minimax criterion is then extended to the selection of optimal absorber parameters for damping two-DOF systems. Finally, the minimum cost criterion is applied to the simultaneous and sequential optimizations of the passive components of an actuator and the active feedback gains.

Optimal Absorber Design for a One-DOF Structure

Steady-State Solution

The first optimality criterion is to minimize the maximum steady-state response x_1 when the structural mass m_1 is subjected to a white noise disturbance P. The nondimensional transfer function relating input disturbance to response for the model in Fig. 1b is

$$\left|\frac{x_1}{P/k_1}\right|^2 = \frac{4\mu^2\gamma^2 + (\gamma^2-\delta^2)^2}{[\beta\delta^2\gamma^2 - (\gamma^2-1)(\gamma^2-\delta^2)]^2 + 4\mu^2\gamma^2[\gamma^2(1+\beta)-1]^2} \quad (1)$$

where

$\delta = [(k_2/m_2)/(k_1/m_1)]^{1/2}$ absorber/structure frequency ratio (2a)

$\gamma = \omega/(k_1/m_1)^{1/2}$ nondimensional frequency ratio (2b)

$\beta = m_2/m_1$ absorber/structure mass ratio (2c)

$\mu = c/2m_2(k_1/m_1)^{1/2}$ nondimensional damping (2d)

The solution based upon minimization of the maximum steady-state response, known as the "Classical Vibration Absorber" problem,[1] is summarized here. The maximum response of the structural mass m_1 with an optimally tuned absorber attached is

$$\left.\frac{x_1}{P/k_1}\right|_{\max} = \left[\frac{2+\beta}{\beta}\right]^{1/2} \quad (3)$$

It is clear that increasing the absorber/structure mass ratio β lowers the response. Therefore, increasing the absorber mass improves performance, and no "optimal" mass ratio exists. Therefore, the mass ratio β is assumed fixed, and the values of the frequency ratio δ and nondimensional damper μ are optimized.

For a fixed-mass ratio, the optimal frequency ratio δ_{ss} based on the minimax criterion is

$$\delta_{ss} = 1/(1+\beta) \quad (4)$$

and the optimal nondimensional damper setting is found by solving

$$\mu_{ss}^2 = \frac{(\delta_{ss}^2-\gamma_{ss}^2)^2 - [\beta\delta_{ss}^2\gamma_{ss}^2 - (\gamma_{ss}^2-1)(\gamma_{ss}^2-\delta_{ss}^2)]^2(x_1k_1/P)^2}{4\gamma_{ss}^2[\gamma_{ss}^2(1+\beta)-1]^2(x_1k_1/P)^2 - 4\gamma_{ss}^2} \quad (5)$$

where the nondimensional modal frequencies are

$$\gamma_{ss}^2 = \frac{1}{1+\beta}\left\{1 \mp \left[\frac{\beta}{2+\beta}\right]^{1/2}\right\} \quad (6)$$

Equation (5) is indeterminate at these modal frequencies γ_{ss}. To determine μ_{ss}, a limit of Eq. (5) must be taken for values of γ approaching γ_{ss}.

A numerical example of this steady-state solution is shown in Fig. 2 for a mass ratio of $\beta = 0.02$ (i.e., the absorber mass m_2 is 2% of the structural modal mass m_1) and for the optimal frequency ratio of $\delta_{ss} = 0.98$. Given this mass and frequency ratio, Fig. 2 shows the response to white noise excitation for six nondimensional damper settings. Notice that $\mu = 0.08$

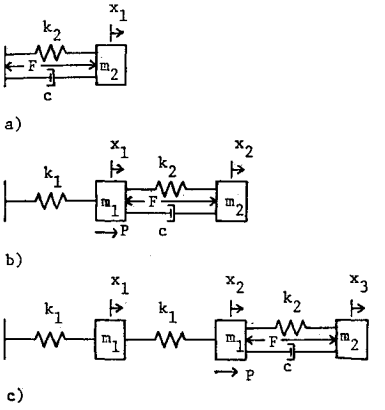

Fig. 1 a) A 1-DOF absorber/actuator coupled to b) a 1-DOF structure and c) a 2-DOF structure.

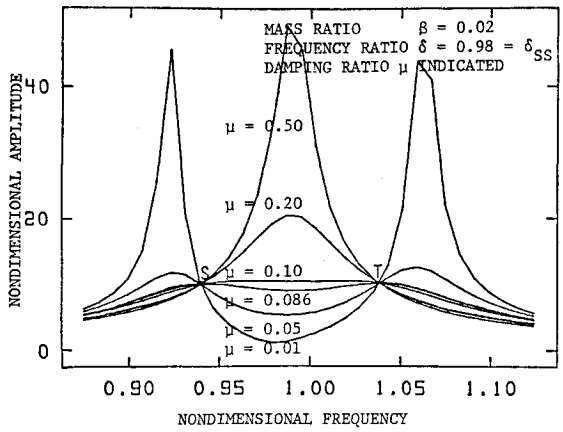

Fig. 2 Response (x_1k_1/P) vs frequency $[\omega/(k_1/m_1)^{1/2}]$ for the system of Fig. 1b for the optimal frequency ratio, the given mass ratio, and the indicated damping.

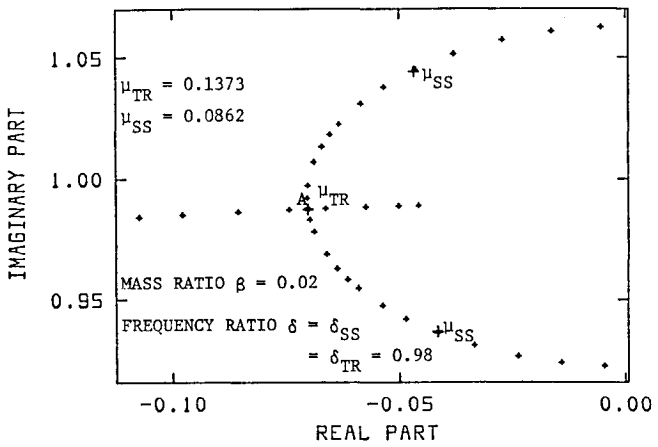

Fig. 3 S-plane representation of the poles of Fig. 1b as a function of increasing damper value.

appears to minimize the maximum response and in fact corresponds to μ_{ss} derived using Eq. (5).

Transient Response Solution

The criterion used to determine the optimal transient response solution is that of minimizing the maximum modal time constant. Figure 3 shows the root locus for the system of Fig. 1b as the damper μ is varied (for a mass ratio of $\beta = 0.02$). The frequency ratio δ has been chosen such that the root trajectories intersect at point A. This allows both poles to be moved as far to the left as possible. This optimal value of δ_{TR}, which causes the loci to intersect at point A, is the same as that calculated using Eq. (4). The optimal damping that places both poles at point A is

$$\mu_{TR}^2 = \beta/(1+\beta)^3 \tag{7}$$

The real part of the poles at point A is

$$RE(s)\Big|_A = -0.5[\beta/(1+\beta)]^{1/2} \tag{8}$$

As in the steady-state response optimization, optimum performance improves monotonically for increasing β. For the numerical example of $\beta = 0.02$, $\delta_{ss} = \delta_{TR} = 0.98$ [Eq. (4)], the optimal damper is $\mu_{TR} = 0.137$ [Eq. (7)], which is 60% larger than the value for μ_{ss} derived using the steady-state minimax criterion [Eq. (5)]. Figure 3 also shows the pole locations for the system with the optimal steady-state response ($\delta = \delta_{ss} = \delta_{TR}$ and $\mu = \mu_{ss}$). In general, lower damping is required for optimal steady-state response than for optimal transient response.

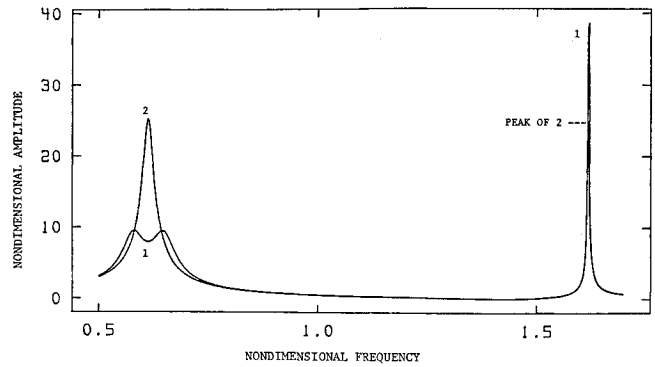

Fig. 4 Response (x_1k_1/P) vs frequency $[\omega/(k_1/m_1)^{1/2}]$ for the system of Fig. 1c for the choice of damping that minimizes the responses of the lower two modes (curve 1) and all modes (curve 2).

Minimum Quadratic Cost Solution

The final optimality criterion for passive absorbers is to minimize a cost function that penalizes the undesirable system response. To be consistent with optimal regulator theory, the quadratic cost function is

$$J = \frac{1}{2}\int_0^\infty [x^TQx + u^TRu]\,dt \tag{9}$$

where x contains the states of the system of Fig. 1b and Q is a positive semidefinite square matrix. In this problem there are no active forces, so that the cost depends only on the quadratic of x, i.e., $R = 0$. For a given Q and initial state vector x_o, a unique solution for a minimum of J can be found by solving the Lyapunov equation for the system.[6] A closed-form analytic solution for this problem has been found for the case of a vibration absorber attached to a one-DOF system.[2] This solution yields the same optimal frequency ratio δ_{ss} and a similar damping level μ as was found previously for the steady-state optimization.

For this analysis, which preceded that of Ref. 2, a numerical search is used to determine the values of frequency ratio δ and nondimensional damper μ that result in the lowest cost J for a fixed mass ratio β. The weighting matrix Q is selected so that the cost J represents the sum of the system's total nondimensional kinetic plus potential energy. Choice of the initial condition x_o does not significantly affect the results for a lightly damped system.

Optimal solutions using the three methods were compared[7] and found to have identical frequency ratios and similar nondimensional dampers. Thus, all three design techniques yield virtually identical absorber designs, particularly with respect to the achievable tuning accuracy of these devices.

Optimal Absorber Design for a Two-DOF Structure

The possibilities of adding damping to several modes through the use of a single absorber are demonstrated by extending the steady-state solution to the design of an absorber for a two-DOF structure (Fig. 1c). Once again, the objective is to minimize the maximum steady-state response at the disturbance location. For a structure with multiple DOF's, no simple closed-form solution, such as Eqs. (4) and (5), is known. A nonrigorous extension of the single-DOF absorber analysis is presented.

The optimization possibilities are summarized in Fig. 4, where the frequency response of the system in Fig. 1c is shown for two sets of passive absorber parameters. Again, the mass ratio is fixed at $\beta = 0.02$, where β is now defined as the ratio of absorber mass to modal mass of the lower structural mode. Curve 1 shows the absorber tuned to the lower structural mode using the relations given in Eqs. (4) and (5) altered to refer to modal properties. In this case the absorber parameters yield a

suboptimal result because the response at the high mode frequency is about four times larger than the response of the lower two modes. Increased absorber damper strength reduces apparent damping in the lower two modes while increasing residual damping in the high mode. The term "apparent damping" refers to the damping exhibited by the combined steady-state response of two split modes that occur at almost identical frequencies. With sufficient additional damping the two peak amplitudes are equated and the minimax criterion is again satisfied (Curve 2).

The absorber frequency can also be tuned to the higher structural mode. However, this choice of absorber frequency is inappropriate. When the absorber frequency is tuned to the higher mode, no value of the damper can be found that equates the response of the two structural modes. It is therefore important that, when attempting to introduce significant levels of damping into more than one structural mode, the absorber frequency be tuned to the frequency of the lowest mode of interest and the damper increased from the value determined by Eq. (5) until the desired damping in the higher modes is achieved. The validity of this approach was independently confirmed by a quadratic cost minimization approach.[7]

Optimization of Passive Components of an Active Actuator

The next step in the study of inertial reaction devices is to determine the optimal passive components of the active control actuator shown in Fig. 1a. The control force F is assumed to be a linear function of the displacement and velocity states of both the structural mass m_1 and the actuator m_2 of Fig. 1b, i.e., full-state feedback. Both the active feedback gains and the values of the passive components are optimized simultaneously. The objective of this optimization is to determine what similarity these passive parameters bear to the optimal parameters of the passive vibration absorber.

The method used for the simultaneous optimization of the active feedback gains and passive parameters is similar to the previously discussed quadratic cost minimization [Eq. (9)]. The quadratic cost now includes a penalty on the control effort, so that R is a positive, dimensionless constant. By the choice of $R = 100$, the level of control forces are kept to the same order of magnitude as those generated by the passive components. This is done to prevent domination of the actuator dynamics by either the passive components or active forces. Since a tuned absorber provides significant passive damping in the tuned mode, at a relatively low mass ratio, the addition of active control forces of the same order of magnitude would provide damping performance well within the level necessary for typical applications.

To simultaneously optimize the passive components and active gains, a gradient search is performed for a range of values of the actuator's passive frequency ratio δ and nondimensional damper μ. For each δ and μ, the optimal regulator gains are calculated exactly from regulator theory and the cost evaluated [(Eq. (9)]. Note that no penalty is explicitly placed on the passive components, and therefore, the optimal solution will be driven toward relying as heavily as possible on the passive components of the actuator.

The two systems that were optimized for the passive vibration absorber (Figs. 1b and 1c) were also optimized for the active actuator.[7] One characteristic result throughout the optimizations was that the optimal δ for the actuator is near the optimal δ_{ss} of the passive vibration absorber. The optimal value of the damper μ is somewhat more sensitive to the presence of active feedback and therefore deviates from the optimal for an absorber by a greater percentage than do the frequency ratios.

The results of the simultaneous optimization suggest that sequentially optimizing first the passive components and then the active gains will yield nearly the same performance. This indicates that the inertial reaction control actuator performs most effectively when passively tuned as a vibration absorber. Supplemental passive damping is added to the system, and actuation effectiveness is increased.

Table 1 Brass beam and suspension characteristics

Length	$l = 7.315$ m
Width	$b = 0.102$ m
Thickness	$t = 0.003$ m
Mass density/unit length	$m = 4.12$ kg/m
Bending stiffness	$EI = 30.0185$ N m^2
Suspension cable length	$L = 2.450$ m

Mode	Frequency (Hz)	Damping ratio
1	0.300	—
2	0.320	—
3	0.368	0.0057
4	0.632	0.0032
5	1.120	0.0021
6	1.820	0.0018
7	2.760	0.0014
8	3.840	0.0016
9	5.200	0.0014
10	6.640	0.0015
11	8.320	0.0016
12	10.160	0.0017

Experiments Using Inertial Reaction Control Actuators

In order to investigate the practical implementation and limitations of space-realizable active control, an extensive set of experiments was conducted. The experimental objective was to maximize the damping in a pendulous free-free beam. After a description of the experimental hardware and open-loop plant model, the results for the test in which the inertial reaction devices were experimentally tuned as passive vibration absorbers to various beam modes are discussed. Once tuned, these devices were used as active actuators through the feedback of system measurements. Finally, the performance of these controllers is compared to the performance of untuned and non-space-realizable actuators.

Experimental Apparatus

Control Hardware

The structural plant of a prototypical space structure can be characterized as having free boundary conditions and a low-frequency fundamental mode. Such conditions raise issues concerning actuator stroke limitations and low-frequency stiction effects. This behavior was simulated by a 24-ft brass beam suspended by wires arranged in six sets of swinging parallelograms (Fig. 5a), which prohibited torsional rotation about the beam's longitudinal axis. The first bending mode of this free-free structure was at 0.37 Hz. The pendulous modes were at 0.30 and 0.32 Hz. The small frequency separation between the pendulous and first bending modes was due to a desire to make the flexible modes as low as possible, but above the pendulum modes, while being restricted by suspension length. The system had four modes below 1.0 Hz and eleven modes below 10.0 Hz (Table 1), providing the experimental challenge of close modal spacing. Typical open-loop modal damping ratios averaged 0.16% of critical ($\zeta = 0.0016$).

Four identical, space-realizable, electromagnetic, inertial-reaction actuators, with characteristics as listed in Table 2, were used to control the structure (Fig. 5b). These devices, which are variations of devices developed at the Lockheed Palo Alto Research Laboratory,[3] were attached to the side of the beam and used a commanded motor torque to accelerate a pivoting reaction arm through small angle deflections. This caused the proof-mass, attached to the end of the pivoting arm, to accelerate horizontally in a direction transverse to the beam. At the point of attachment of the actuator to the beam, this motion generated a reaction force and a small reaction

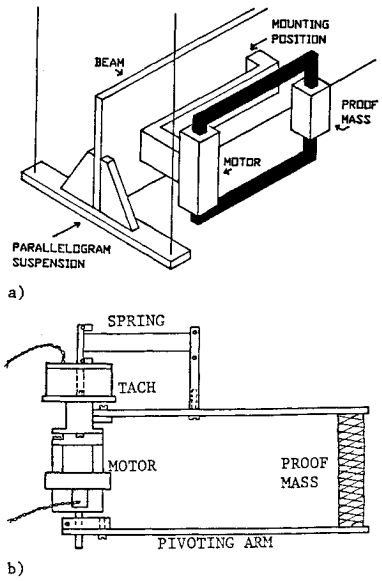

Fig. 5 a) Schematic of parallelogram beam suspension and actuator attachment and b) detailed view of inertial reaction absorber/actuator.

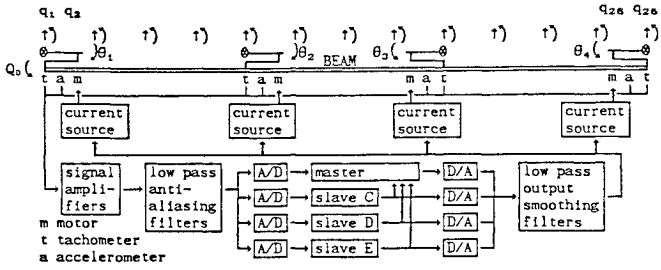

Fig. 6 Control hardware configuration and modeled DOF's for the experiment.

torque, both of which had to be modeled.[8] An adjustable spring was included to enable adjustment of the natural frequency of each device, and colocated feedback of motor shaft rate to motor torque was locally fed back to simulate a passive damper, thus allowing the devices to be used as both tunable vibration absorbers and control actuators with tunable passive components. The active damper provided simple damping adjustment and linearity and, in principle, could be replaced with a truly passive mechanism such as constrained viscoelastic layers in the adjustable spring. Therefore, for the remainder of this paper, the adjustable spring and locally fed-back colocated, electronic damper will be referred to as passive elements of the device. A momentum wheel was attached to one end of the beam to provide either broadband disturbance torque used in transfer function tests or sinusoidal disturbance torques used to initiate free decay tests.

Eight space-realizable sensors were used to estimate system states. Each actuator contained a tachometer for measuring relative pivoting arm rotation rate. At the location of each actuator, an accelerometer was used to measure coincident inertial beam acceleration (Table 2). The beam and actuator positions and velocities at each actuator location were estimated from the tachometer and accelerometer measurements by a digital algorithm that filters low-frequency signal drift and integrates the measurements over a frequency range encompassing the system modes of interest.[9]

Discrete time processing was accomplished in one master and three slave 8088/8087 processors with each of the four processors devoted to controlling a separate actuator. Measurement information was exchanged between processors through dual-access, shared memory space. Analog-to-digital and digital-to-analog conversion was used by each processor for sensor sampling and issuing control commands at a rate of 1000 Hz. This high control rate allowed feedback gains to be derived based on the assumption of continuous control for modes up to 10 Hz. Double-precision operations were used to prevent roundoff errors in the integration and control algorithms. The details of the digital hardware are listed in Table 3. Once this equipment was assembled as illustrated in Fig. 6, a mathematical model of the system was constructed and verified.

System Model

A finite-element model consisting of twelve cubic beam elements and augmented by the dynamics of the four actuators was formulated using the DOF's indicated in Fig. 6. The model was first formulated with only the 26 beam degrees of freedom plus the mass and disturbance torque Q_D of the momentum wheel and the stiffness of the suspension system. Very slight changes in the beam cross-sectional stiffness were made so that this model accurately represented the experimentally observed open-loop beam behavior. Then the actuators, with springs set very stiff, were physically added to the beam and mathematically added to the model. Modal damping was then experimentally determined for each mode and added to complete the mathematical model of the form

$$\begin{bmatrix} \begin{bmatrix} 0 & \\ F & E \\ 0 & M \end{bmatrix}_{26\times 26} & \begin{matrix}\text{Actuator}\\ \text{coupling}\\ \text{to beam}\end{matrix} \\ \text{Actuator dynamics} & \end{bmatrix}_{30\times 30} \begin{bmatrix} \ddot{q}_1 \\ \vdots \\ \ddot{q}_{26} \\ \ddot{\theta}_1 \\ \vdots \\ \ddot{\theta}_4 \end{bmatrix}_{30\times 1} + \begin{bmatrix} \begin{bmatrix} 0 & \\ F & E \\ 0 & M \end{bmatrix}_{26\times 26} & \begin{matrix}\text{Actuator}\\ \text{coupling}\\ \text{to beam}\end{matrix} \\ \text{Actuator dynamics} & \end{bmatrix}_{30\times 30} \begin{bmatrix} \dot{q}_1 \\ \vdots \\ \dot{q}_{26} \\ \dot{\theta}_1 \\ \vdots \\ \dot{\theta}_4 \end{bmatrix}_{30\times 1}$$

$$+ \begin{bmatrix} \begin{bmatrix} 0 & \\ F & E \\ 0 & M \end{bmatrix}_{26\times 26} & \begin{matrix}\text{Actuator}\\ \text{coupling}\\ \text{to beam}\end{matrix} \\ \text{Actuator dynamics} & \end{bmatrix}_{30\times 30} \begin{bmatrix} q_1 \\ \vdots \\ q_{26} \\ \theta_1 \\ \vdots \\ \theta_4 \end{bmatrix}_{30\times 1} = \begin{bmatrix} Q_1 \\ \vdots \\ Q_{26} \\ \tau_1 \\ \vdots \\ \tau_4 \end{bmatrix}_{30\times 1} + \begin{bmatrix} 0 \\ Q_D \\ 0 \\ \vdots \\ 0 \end{bmatrix}_{30\times 1} \tag{10}$$

With this refined model, the first 17 predicted open-loop modal frequencies of the beam, plus stiff actuators, were within 2% of their measured values. The final actuator stiffnesses and damper strengths used in the model were determined during the actuator tuning process.

In each of the following experiments, two types of tests were performed. First, the acceleration transfer function from broadband disturbance torque at one end of the beam ($Q_D = 0.006$ Newton meters rms) to linear transverse beam acceleration at the other end was recorded via a spectrum analyzer. Second, the beam was excited at individual modal frequencies and allowed to undergo free decay after shutdown

Table 2 Force actuator specifications and components

Maximum actuator force	3.0	N
Actuator mass w/o proof-mass	0.550	kg
Proof-mass mass	0.165	kg
Pivoting arm length	0.127	m
Motor peak amperage	4.920	A
Motor peak voltage	19.10	V
Torque constant	35.70	mN m/A
Peak stall torque	173.0	mN m
DC motor	Pittman Corp. Model 7214	
Tachometer	Inland Motor Model TG-0702	
Accelerometer	Endevco Piezoresistive Model 2262-25	

Table 3 Digital control hardware

Master system		
Packaging:		LabTech
CPU:	JF Microsystems	Model 8759 8088/8087 8-bit STD bus
A/D:	Analog devices	Model RTI-1260 8 differential channels +/− 10 V 12-bit conversion 25-μs conversion time
D/A:	Analog devices	Model RTI-1262 4 channels +/− 10 V 12-bit conversion 25-μs settling time
Slave system		
CPU:	Ziatech	Model ZT 8830 8088 8-bit STD bus
A/D:	Intel	Model iSBX 311 8 differential channels +/− 5 V 12-bit conversion 50-μs conversion time
D/A:	Intel	Model iSBX 328 8 channels +/− 5 V 12-bit conversion 20-μs settling time
High speed math board:	Intel	Model iSBX 331 FMUL 50 μs

of the excitation while beam end acceleration was measured. The modal damping ratios were calculated from these transient decays.

Tuned Passive Absorber Experiments

The first set of experiments involved tuning the four actuators, used as passive absorbers, to four "target modes" of the beam and determining their effectiveness as passive absorbers. Modes targeted for absorber tuning were those most sensitive to the disturbance. Equation (11) defines the modal transmission from disturbance to regulated variables for lightly damped systems in the form of Eq. (12) as derived by internal balancing theory.[10] For this experiment, the regulated variables y have been chosen to be the entire state vector x, i.e., it is desirable to minimize the disturbance to all of the physically scaled state variables equally. This selects the modes with the largest energy content.

$$\sigma_{DC_i}^2 = (4\zeta_i\omega_i)^{-1}[d_i d_i^T(\omega_i^{-2} + 1)c_{1i}^T c_{1i}]^{1/2} \tag{11}$$

$$\dot{x} = Ax + Bu + Dw \quad \text{state equation}$$

$$z = Mx \quad \text{measurement equation}$$

$$y = Cx \quad \text{regulated variable equation}$$

$$u = -Fz \quad \text{feedback equation} \tag{12}$$

In Eq. (11), ω_i is modal frequency, ζ_i is modal damping, and c_{1i} and d_i are columns and rows of the regulated variable matrix C and disturbance matrix D, respectively.

Figure 7 shows with hatched bars the transmission, as defined by Eq. (11), from the disturbance to the regulated variables for the first 13 open-loop modes. The result of the presented analysis, in which an absorber is tuned to more than one degree of freedom, indicates that it is desirable to tune to the lower-frequency modes of interest. Therefore, the four lowest consecutive modes with high disturbance transmission were chosen as the target modes, as shown by the arrows in Fig. 7. The four absorbers had been placed at positions along the beam where they exerted a large influence on their respective target modes due to large modal motion, i.e., the absorbers were placed in positions that maximized the modal mass ratio [Eq. (2c)]. One absorber was placed at each end and one was placed at each one-third-length position (Fig. 6).

One absorber was tuned to each of the four target modes. The optimal passive absorber stiffness and damping were chosen using the steady-state minimax criterion [Eqs. (4) and (5)]. The mechanical spring in the actuator was adjusted as accurately as possible to the optimal frequency, and the colocated feedback of actuator rotational position and rate was used to fine-tune the devices. While this does not result in a purely passive system, the active part was used only to enable easy tuning and was not necessary to the performance of the absorbers.

The performances and limitations of the four conceptually passive absorbers were then assessed. A qualitative comparison of the acceleration transfer function of the beam is shown in Fig. 8. Two traces are shown, one for the case of very stiff absorbers such that there is relatively little motion across the dampers (a), and the second for the case of tuned absorbers (b). The four target modes are those with frequencies of 1.09, 1.74, 2.61, and 3.78 Hz. Note the reduced response (increased modal damping) in this frequency range as a result of absorber tuning. Additional, or residual, damping is also evident in the modes above 4.0 Hz. The existence of residual damping in modes higher than the modes to which the absorbers are tuned is consistent with the observations made from the two-DOF tuning analysis (Fig. 4).

The second set of tests involved transient decays of the target modes, the results of which are summarized in Table 4. As can be seen by comparison of the modal damping ratios before and after tuning, over an order of magnitude increase in critical damping ratio was achieved. Sixty to ninety percent of the predicted damping was obtained. Due to the second-order dynamics of the absorbers, tuning to a target mode results in two split modes close in frequency to the original target mode frequency (e.g., target mode 5 becomes modes 5a and 5b). The damping ratio of the more lightly damped mode is reported in Table 4. The deviation between actual and predicted damping in target mode 5 was due to friction effects. Stiction would seize the actuator motion at low vibration levels causing marked reductions in damping and limiting low-amplitude performance. The low performance in mode 8 was due to the low mass ratio, which increased tuning sensitivity and difficulty. In general, the absorbers could not

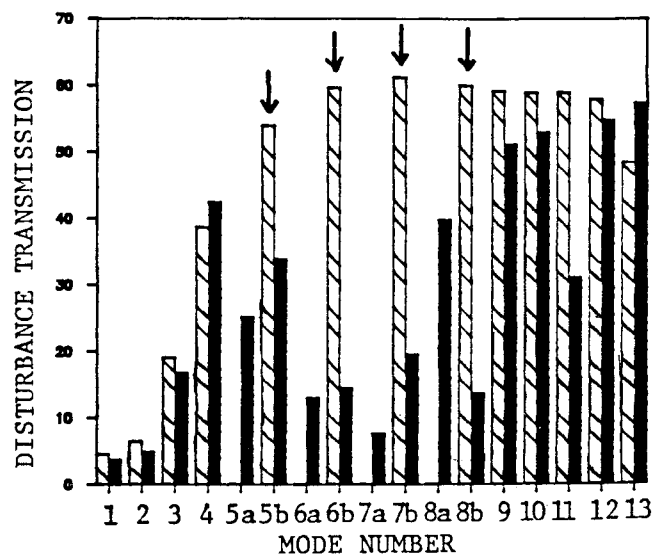

Fig. 7 Level of disturbance transmission to the model states for the system without (hatched) and with (solid) absorbers tuned to target modes.

be tuned to modes lower than 1 Hz due to stiction problems and prohibitively large tuned absorber motion.

Several beneficial characteristics occur as a result of absorber tuning. Figure 7 shows that predicted modal disturbance transmissions are significantly reduced [Eq. (11)] for the beam with tuned absorbers (solid bars) when compared to those for the beam without tuned absorbers (hatched bars). Due to split-mode behavior, two solid bars occur for each of the four hatched bars corresponding to the original target modes 5-8.

Controllability of the target modes is also enhanced by tuning (Fig. 9). The modal control transmission from actuator to regulated variables is defined by internal balancing theory,[10] in a fashion similar to disturbance transmission, as

$$\sigma_{BC}^2 = (4\zeta_i\omega_i)^{-1}\,[b_i b_i^T(\omega_i^{-2}+1)c_{1i}^T c_{1i}]^{1/2} \qquad (13)$$

The vector b_i corresponds to a row of the control effectiveness matrix B. Since these values indicate the effect of control action on the states of the system, they are good indicators of relative modal controllability. Note that the split-target modes are most controllable. The next most controllable modes are the beam modes above the target modes. Modes lower than the target modes are relatively uncontrollable.

Significant increases in passive damping have been achieved by the addition of the passive absorbers. If these same devices are also used as active actuators, it can be argued that the damping is introduced with no additional mass penalty. While the benefits of adding passive absorbers are substantial, the limitations are also important. Friction poses a problem in damping low-level vibrations where stiction can seize absorber motion. This might be overcome with a high-frequency torque dither, which might excite unwanted high-frequency response, or through bearing improvement. Stroke limitations hinder tuning to low-frequency modes at low mass ratios. Finally, passive tuning of the absorbers requires a precise knowledge of the target mode frequency.

Active Control Experiments

Once the actuators had been passively tuned as absorbers to the four target modes, three sets of control experiments were performed using negative output feedback [Eq. (12)]. First, dual rotational rate feedback was used to drive the dc motors of the four tuned actuators from the four tachometers using a fully populated, positive definite gain matrix F. Dual feedback refers to like-sensor-to-like-actuator feedback (rotational shaft rate to shaft torque) where each sensor is physically located with an actuator.[5] In the second set of tests, the same dual measurements were fed back to untuned, zero-stiffness actuators. This verified the effectiveness of tuning the actuators as absorbers with nonzero stiffness. Finally, a control test was performed using one actuator reacting against the laboratory frame. This demonstrated the performance differences between space-realizable and non-space-realizable experiments.

Dual Feedback to Tuned Actuators

Two different tests were performed using positive definite, dual feedback as derived using the technique described in Ref. 5. In this technique, a matrix D_c is chosen to be a positive definite, diagonal matrix whose entries are the desired increases in damping for a chosen set of modes equal in number to the number of actuators used. In this experiment, equal damping was desired such that $D_c = \alpha I$. Next, the modal eigenvector matrix of the full system model is decimated while retaining rows corresponding to actuator motion and columns corresponding to the chosen set of modes. This decimated matrix is designated as Φ_{DEC}. The feedback gain matrix is then derived as

$$F = \Phi_{DEC}^{-T} D_c\, \Phi_{DEC}^{-1} \qquad (14)$$

The quadratic form of Eq. (14) guarantees a positive definite feedback matrix.

The two tests that were performed differed in the four modes chosen to form Φ_{DEC}. The first test used the lowest two target modes, to which actuators were tuned, and their two corresponding split actuator modes (5a, 5b, 6a, and 6b) to create Φ_{DEC}. The second test used the first four beam modes above the target modes (modes 9, 10, 11, and 12) to create Φ_{DEC}.

When the lowest two target and their corresponding actuator modes were chosen to derive the feedback through

Table 4 Experimental results of absorber tuning

Target mode number	5	6	7	8
Target mode frequency (Hz)	1.09	1.74	2.61	3.78
Absorber/modal mass ratio	0.033	0.011	0.018	0.004
Optimal frequency ratio	0.968	0.990	0.983	0.996
Optimal nondimensional damper	0.111	0.062	0.079	0.039
Predicted critical damping ratio	0.0637	0.0362	0.0470	0.0231
Measured critical damping ratio	0.0441	0.0320	0.0438	0.0136
% Achievement (measured/predicted)	69.2%	88.4%	93.2%	59.0%
Damping ratio prior to tuning	0.0021	0.0018	0.0014	0.0016
Increase in critical damping ratio	21	18	31	9

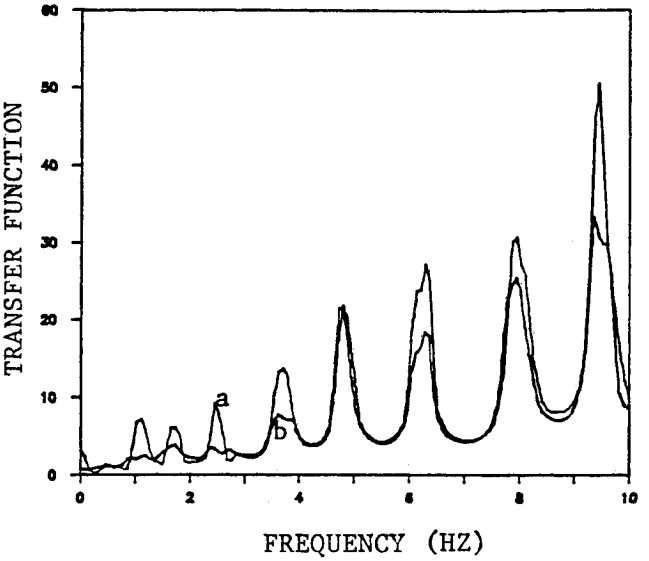

Fig. 8 Acceleration transfer function a) with very stiff absorbers (higher-level response) and b) with tuned absorbers (lower-level response).

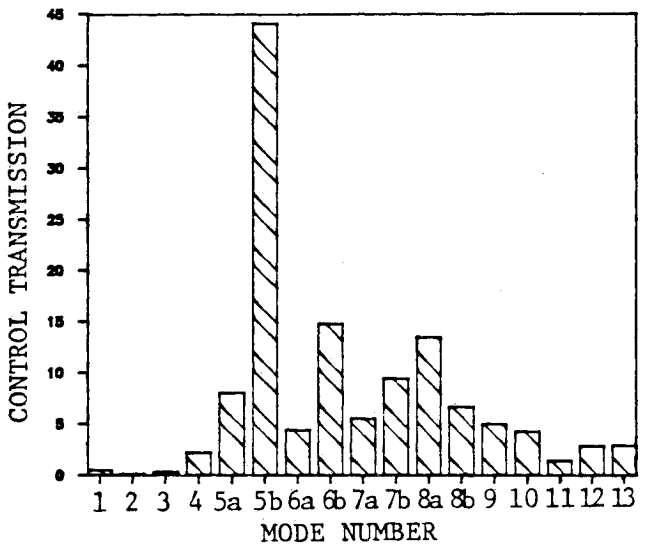

Fig. 9 Level of control transmission to the model states for the system with absorbers whose passive components are tuned to those of an optimal absorber.

Eq. (14), a feedback matrix resulted which contained highly nonuniform entries. This was due to the relatively large eigenvector entries corresponding to the motion of the two actuators tuned to these two lower target modes (5 and 6). The inversion of the decimated eigenvector matrix Φ_{DEC} in Eq. (14) resulted in high feedback gains for the two actuators not tuned to these two lower target modes (i.e., the actuators tuned to modes 7 and 8). The highest gain loop was colocated feedback to the actuator which had been tuned to target mode 8. This gain was four orders of magnitude larger than the colocated feedback to the actuator tuned to target mode 5. Because of the nonuniform gain matrix, this design only created significant feedback to actuators tuned to the higher two target modes (7 and 8).

Using this feedback, only minor increases in damping in modes 9 and 10 (at 4.95 and 6.42 Hz) above the target modes occurred at the expense of damping in target mode 8 (at 3.78 Hz) of the beam/actuator system. Table 5 lists measured and predicted closed-loop modal characteristics for this test for the feedback gain level chosen. The model and the data are in fair agreement. This behavior can be explained using Fig. 3 to represent the root locus in the vicinity of mode 8. Above a certain level of positive colocated rate feedback, that which places the poles at the equivalent of point A, one of the root trajectories for modes 8a and 8b moves toward the imaginary axis. This results in reduced apparent damping in that mode. Recall that the colocated rate feedback to the actuators tuned to modes 7 and 8 dominate the feedback gain matrix. The model did not predict reductions in modal damping, due to the feedback, at this gain level but did so at a slightly higher gain level.

An important limitation was realized through this test. The feedback used was at a level just below that which caused the onset of a high-frequency (67 Hz) instrumentation/actuator instability, similar in nature to those reported in Ref. 11. Only relatively low-control performance was achieved prior to the onset of this instability. Due to the nonuniform gain matrix, the relatively high gains to one actuator caused a local instability before significant control authority could be exerted overall. The corrective step was to create a more uniform feedback matrix while retaining the desirable positive definite, dual feedback properties.

In the second test with dual feedback to tuned actuators, Eq. (14) was again used to derive a feedback matrix using an eigenvector transformation Φ_{DEC} based on the first four beam modes above the target modes (i.e., modes 9, 10, 11, and 12). Uniformity in the gain matrix was achieved since the actuator eigenvector entries were of similar magnitudes. Figure 10 compares the acceleration transfer function of the beam with only the tuned absorbers (a) to that of the beam with additional uniform feedback to tuned actuators (b). Significant increases in damping in modes 9–12 resulted at a cost of only slight reductions in apparent damping in target modes 5–8 (note the hatching in Fig. 10). Table 5 lists the predicted and measured modal characteristics. As can be seen in both Fig. 10 and Table 5, modes 9 and 10 received the largest increases in damping. Better performance was achieved in this case because all four actuators were contributing evenly. In fact, all modes above 4 Hz exhibited significant increases in damping. Again, an instrumentation/actuator instability limited the feedback gain level. This result verifies that uniform feedback provides better performance since it allows all actuators to contribute before the onset of instability.

Several conclusions can be drawn from this first set of two tests. Nonuniform feedback resulted in poor performance while uniform feedback allowed significant increases in higher mode damping at the slight sacrifice of modal damping in the target modes to which the actuators were tuned. The active feedback, while introducing additional damping, also redistributes the damping in the target modes across a wider spectrum. In both tests, positive definite dual feedback proved stable with respect to beam modes for all gain levels tested up to that which caused instrumentation/actuator instability. This type of feedback also guarantees an increase in total system damping but does not necessarily guarantee simultaneous damping increases in all modes at all gains.

Dual Feedback to Untuned Actuators

In the next set of experiments, the same type of dual-rate feedback [Eq. (14)] was used in conjunction with untuned, almost zero-stiffness actuators. This was done to illustrate the benefits of tuning to plant modal frequencies in the range over which control is desired. As in the previous case, the feedback was increased until the onset of instrumentation/actuator instability. Table 6 lists the results for modes 5–12 at the highest stable gain level used. Note that the split modes associated with the dynamics of the actuators have now disappeared since the actuator stiffnesses have been set essentially to zero. The results in Table 6, when compared to Table 5, verify that actuator tuning yields improved performance. To obtain the same response characteristics, a controller providing position and rate feedback would have to have active gains to the untuned actuators that provide the passively generated reactions that exist in the tuned actuator case.

Non-Space-Realizable Actuation

The last test involved a non-space-realizable method of control actuation in which one actuator reacted against the laboratory wall instead of the proof-mass at the end of the pivoting arm. In this case, the simple colocated actuator rate was negatively fed back to the actuator. Figure 11 compares

Table 5 Test results for nonuniform and uniform positive definite dual feedback to tuned actuators

			Nonuniform			Uniform		
Mode number	Frequency, Hz	ζ Open-loop (measured)	Closed-loop (predicted)	Closed-loop (measured)	% measured predicted	Closed-loop (predicted)	Closed-loop (measured)	% measured predicted
5a	1.05	0.0441	0.0441	—		CRIT	—	
5b	1.27	—	0.0479	—		0.0233	—	
6a	1.72	0.0320	0.0329	—		0.8635	—	
6b	1.88	—	0.0382	—		0.0470	—	
7a	2.49	—	0.0709	—		0.7144	—	
7b	2.75	0.0438	0.0715	—		0.0546	—	
8a	3.69	0.0136	CRIT	CRIT		0.4131	—	
8b	3.95	—	0.0173	0.0095	54.9%	0.0259	—	
9	4.95	0.0040	0.0055	0.0110	200.0%	0.0155	0.0118	76.0%
10	6.42	0.0033	0.0042	0.0041	97.6%	0.0156	0.0129	83.0%
11	8.19	0.0048	0.0055	0.0047	85.5%	0.0103	0.0084	82.0%
12	9.80	0.0025	0.0029	0.0025	86.2%	0.0075	0.0060	80.0%

— not measured

the acceleration transfer function of the beam with tuned absorbers (a) to that of the beam with one actuator allowed to react against the laboratory frame (b), showing how effective this simple feedback is. The level of feedback was again limited by the instrumentation/actuator instability. As is evident from the data, this simple single-actuator arrangement resulted in much better performance than any of the space-realizable methods, even those using four actuators, because the mass ratio is effectively infinite. This illustrates the need to conduct space-realizable experiments in order to identify important limitations that may be overlooked when performing non-space-realizable tests such as this.

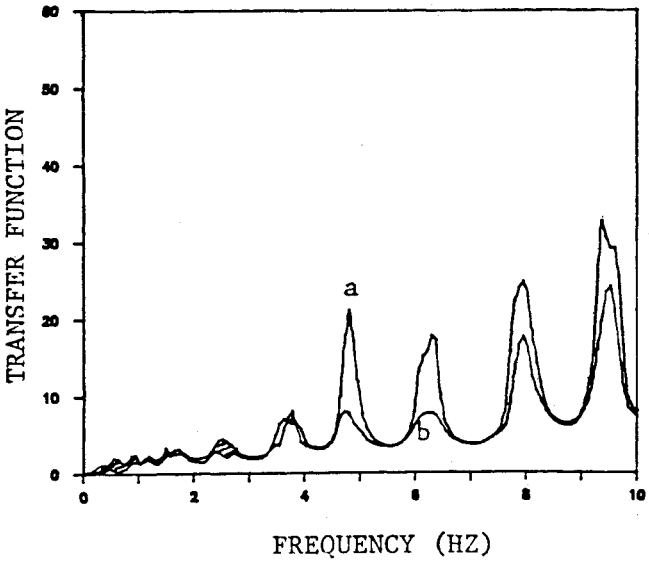

Fig. 10 Acceleration transfer function a) with tuned absorbers (higher-level response) and b) with uniform dual feedback to tuned actuators. Hatching indicates regions in which response is increased in case b.

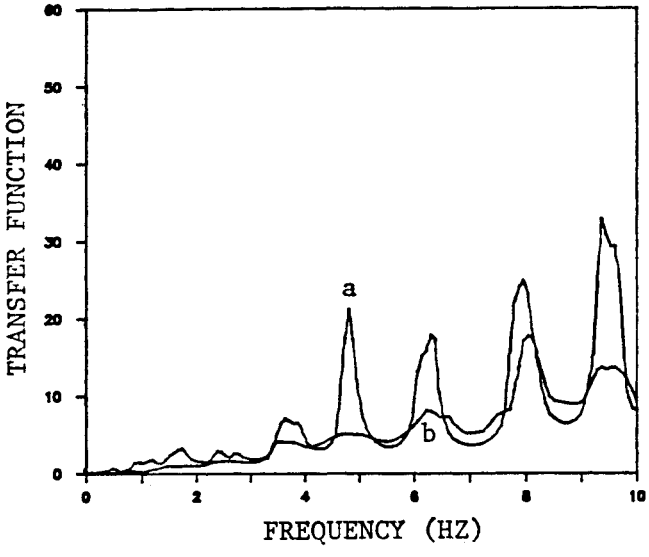

Fig. 11 Acceleration transfer function a) with tuned absorbers (higher-level response) and b) with colocated rate feedback to a single actuator reacting against the laboratory frame (lower-level response).

Table 6 Test results for uniform, positive definite dual feedback to untuned (zero-stiffness) actuators

Mode number	Frequency, Hz	Modal damping ratio Open-loop (measured)	Closed-loop (predicted)	Closed-loop (measured)	% Achievement measured/predicted
5	1.09	0.0021	0.0048	—	—
6	1.74	0.0018	0.0094	—	—
7	2.61	0.0014	0.0056	—	—
8	3.78	0.0016	0.0054	—	—
9	4.92	0.0014	0.0025	0.0018	72%
10	6.40	0.0015	0.0034	0.0031	91%
11	8.19	0.0016	0.0023	0.0017	74%
12	9.79	0.0017	0.0042	0.0030	71%

– not measured

Conclusions

Several conclusions can be drawn from the theoretical optimization of these inertial reaction devices. Three different optimization procedures yielded almost identical absorber designs, providing confidence in the tuning process. In addition, the optimal passive components of the control actuator were found to be similar to those of the optimal absorber. This allows passive damping to be added without significant mass penalty. Finally, when using an inertial device to increase damping in several modes, it is desirable to tune the frequency of the device to the lowest mode and adjust the damping accordingly.

Experimentally, an inertial reaction device was used effectively as both a passive vibration absorber and a control actuator, passively tuned as an absorber, verifying the results of the tuning analysis that stated that passive tuning complements active control. This dual-purpose device resulted in mass savings, increased modal controllability, and reduced target mode disturbance transmission. Additional passive damping increases the gain margin for feedback systems that are conditionally stable and allows a form of passive damping enhancement in the event of control system failure. These space-realizable experiments were found to be important in determining performance limitations due to instrumentation instabilities, friction in relative motion actuators, and actuator saturation at low frequencies. In addition, non-space-realizable tests exhibited excellent damping performance, which emphasized the need to investigate the realistic implementation limitations of space-realizable techniques. Uniformity in the positive definite, dual-feedback matrix allowed better performance before the onset of instrumentation/actuator instabilities because all actuators were able to exert maximum stable feedback.

While the experiments were not able to achieve damping levels needed in proposed space structures (10% critical damping), they did achieve almost half this level in the target modes and increased the damping in the higher modes by almost an order of magnitude. This is typical of the performance required of a low-authority controller with respect to providing significant increases in damping across a frequency range exceeding the bandwidth of the high-authority controller. The corresponding high-authority controller could be implemented using other actuators or using these same devices given that the dual-feedback restrictions set in this paper are relaxed.

Acknowledgments

This research was supported by the Air Force Office of Scientific Research under contract F49620-84-K-0010 with Dr. Anthony Amos as technical monitor.

References

[1]Timoshenko, S., Young, D.H., and Weaver, W. Jr., *Vibration Problems in Engineering*, fourth edition, John Wiley and Sons, New York, 1974, pp. 273-278.

[2]Juang, J., "Optimal Design of a Passive Vibration Absorber for a Truss Beam," *Journal of Guidance, Control and Dynamics*, Vol. 7 No. 6, Nov.-Dec. 1984, pp. 733-739.

[3]Aubrun, J-N., Breakwell, J.A., Gupta, N.K., Lyons, M.G., and Marguiles, G., "ACOSS FIVE (Active Control of Space Structures) PHASE 1A," Lockheed Missiles & Space Co., Inc., Rept. AD-A116655, March 1980-Sept. 1981.

[4]Aubrun, J-N., "Theory of the Control of Structures by Low-Au-

thority Controllers," *Journal of Guidance, Control and Dynamics*, Vol. 3, Sept.-Oct. 1980, pp. 444-451.

[5]Skidmore, G.R., Hallauer, W.L. Jr., "Experimental-Theoretical Study of Active Damping with Dual Sensors and Actuators," AIAA Paper 85-1921; also, *Proceedings of the AIAA Guidance, Navigation and Control Conference*, AIAA, New York, Aug. 1985, pp. 433-442.

[6]Kwakernaak, H. and Sivan, R., *Linear Optimal Control Systems*, Wiley-Interscience, New York, 1972, p. 104.

[7]Miller, D.W., Crawley, E.F., and Ward, B.A., "Inertial Actuator Design for Maximum Passive and Active Energy Dissipation in Flexible Space Structures," AIAA Paper 85-0777; also, *Proceedings of the 26th AIAA/ASME/ASCE/AHS Structures, Structural Dynamics and Materials Conference*, AIAA, New York, April 1985.

[8]Miller, D.W., Ward, B.A., Crawley, E.F., and Widnall, W., "Development of Intelligent Structures Using Finite Control Elements in a Hierarchic and Distributed Control System," Space Systems Laboratory Rept. 1-87, Department of Aeronautics and Astronautics, M.I.T., Air Force Contract F49620-84-K-0010, Final Rept., 1987, Part II, Ch. 5.

[9]Miller, D.W., "Finite Active Control Elements for Large Space Structures," Space Systems Laboratory Rept. 6-85, Department of Aeronautics and Astronautics, M.I.T., 1985.

[10]Gregory, C.Z. Jr., "Reduction of Large Flexible Spacecraft Models Using Internal Balancing Theory," *Journal of Guidance, Control, and Dynamics*, Vol. 7, Nov.-Dec. 1984, pp. 725-732.

[11]Gupta, N.K. et al, "Modelling, Control and System Identification Methods for Flexible Structures," AGARDograph 260, Nov. 1981, pp. 12-13.